PNAS BRIEF REPORT | CELL BIOLOGY OPEN ACCESS

Genetic dissection of intercellular interactions in vivo by membrane-permeable protein

Shaohua Zhang[a], Qianyu Zhang[b], Zixin Liu[a], Kuo Liu[c], Lingjuan He[d], Kathy O. Lui[e], Lixin Wang[f,1], and Bin Zhou[a,b,c,1]

Edited by Roel Nusse, Stanford University School of Medicine, Stanford, CA; received November 18, 2021; accepted November 9, 2022

Unraveling cell–cell interaction is fundamental to understanding many biological processes. To date, genetic tools for labeling neighboring cells in mammals are not available. Here, we developed a labeling strategy based on the Cre-induced intercellular labeling protein (CILP). Cre-expressing donor cells release a lipid-soluble and membrane-permeable fluorescent protein that is then taken up by recipient cells, enabling fluorescent labeling of neighboring cells. Using CILP, we specifically labeled endothelial cells surrounding a special population of hepatocytes in adult mice and revealed their distinct gene signatures. Our results highlight the potential of CILP as a platform to reveal cell–cell interactions and communications in vivo.

genetic tool | intercellular interactions | membrane-permeable protein | liver zonation | niche

Cell–cell interactions are essential to direct cellular behaviors during many physiological and pathological processes (1, 2). Several methods have been reported recently to dissect cell interactions. PIC-seq and ProximID were developed to sort and analyze adjacent cells that are attached to each other (3–5). Based on physical contact, synthetic Notch receptors were also used to label and manipulate the interacting cells (6). Additionally, the Sortase A transpeptidase and FucoID were applied to monitor interactions between T and dendritic cells (7). Furthermore, cell-penetrating fluorescent protein has also been used to label tumor microenvironment in mice by cell transplantation (8). Recently, trans-Tango, TRACT, and BAcTracer have been reported for transsynaptic labeling in drosophila (9–11), providing a flexible platform for neuronal circuit analysis. Despite its importance, a genetic tool that defines and labels neighboring cells of a specific cell type in mammals has yet to be developed.

Results

In principle, lipid-soluble protein (sLP) secreted by donor cells can enter and mark the surrounding recipient cells with a genetic reporter containing a secretary peptide(s) and a transactivator of transcription kappa peptide (8, 12, 13) (Fig. 1 *A* and *B*). To label neighboring cells of defined cell types in vivo, we developed a method termed CILP by generating two knock-in mouse lines, *R26-sLP-mCh-GFP* and *R26-sLP-mCh* (Fig. 1*B*). Therefore, these genetic tools allowed specific sLP-mCherry expression driven under the control of cell type-specific Cre.

For proof-of-concept, we designed liver hepatocytes as donor cells to express sLP-mCherry and GFP and tested whether the nonhepatocytes could serve as recipient cells to be labeled by mCherry. We injected AAV8-TBG-Cre (AAV8-Cre), which specifically targets mouse hepatocytes (14), to *R26-sLP-mCh-GFP* mice and collected their livers for analyses (Fig. 1*C*). Whole-mount analysis revealed that the livers exhibited robust GFP and mCherry expression after AAV8-Cre injection (Fig. 1*D*). It is remarkable to observe that, compared with GFP signal, mCherry was detected in nonhepatocytes as tiny speckles on the liver surface (Fig. 1*D*). In addition to the $GFP^+mCherry^+$ hepatocytes, $GFP^-mCherry^+$ cells were observed in the liver samples, such as endothelial cells, immune cells, and fibroblasts (Fig. 1 *E* and *F*), indicating the transfer of mCherry protein from $GFP^+mCherry^+$ donor hepatocytes to other nonhepatocyte cell lineages. Furthermore, we could also detect the $GFP^-mCherry^+$ recipient cells near the $GFP^+mCherry^+$ donor acinar cells or near the $GFP^+mCherry^+$ donor cardiomyocytes (Fig. 1 *G* and *H*). These examples suggested that CILP could be applied in multiple organ systems.

The liver lobules could be divided into three metabolic zones with distinct properties and molecular markers (14) (Fig. 2*A*). Mfsd2a is a periportal zonation marker (Fig. 2*B*), and $Mfsd2a^+$ hepatocytes can expand and regenerate during injury (15), suggesting the essential role of these subpopulations in the liver. To illustrate the interaction between a subpopulation of hepatocytes and their specific neighboring ECs, we utilized CILP to label ECs that were in the proximity of $Mfsd2a^+$ hepatocytes. We generated *Mfsd2a-CreER;R26-sLP-mCh* mice

Author affiliations: [a]State Key Laboratory of Cell Biology, Center for Excellence in Molecular Cell Science, Shanghai Institute of Biochemistry and Cell Biology, Chinese Academy of Sciences, University of Chinese Academy of Sciences, Shanghai 200031, China; [b]School of Life Science and Technology, ShanghaiTech University, Shanghai 201210, China; [c]Key Laboratory of Systems Health Science of Zhejiang Province, School of Life Science, Hangzhou Institute for Advanced Study, University of Chinese Academy of Sciences, Hangzhou 310024, China; [d]School of Life Sciences, Westlake University, Hangzhou 210030, China; [e]Department of Chemical Pathology, Li Ka Shing Institute of Health Sciences, Prince of Wales Hospital, The Chinese University of Hong Kong, Hong Kong SAR 999077, China; and [f]Department of Cardiac Surgery, Zhongshan Hospital, Fudan University, Shanghai 200032, China

Author contributions: S.Z., Q.Z., Z.L., K.L., L.H., K.O.L., and B.Z. designed research; S.Z., Q.Z., Z.L., K.L., L.H., and K.O.L. performed research; S.Z., L.W., and B.Z. analyzed data; and L.W. and B.Z. wrote the paper.

The authors declare no competing interest.

[1]To whom correspondence may be addressed. Email: wang.lixin@zs-hospital.sh.cn, zhoubin@sibs.ac.cn.

Published December 27, 2022.

in which sLP-mCherry expression was induced after tamoxifen treatment. We found that hepatocytes near the periportal vein expressed mCherry, leading to subsequent labeling of surrounding nonparenchymal cells that included CDH5$^+$ ECs (Fig. 2*C*). The diffusion distance of sLP-mCherry was ~50 μm, which was about 2 to 3 hepatocytes layers in thickness (Fig. 2*D*). Quantification showed that >90% of ECs in zone 1 and ~30% of ECs in zone 2 were mCherry$^+$, while ECs in zone 3 were rarely labeled (Fig. 2 *E* and *F*). For ECs in each zone, there is no significant difference in their labeling efficiency between samples collected at 3 and 6 wk after tamoxifen induction (Fig. 2*F*), suggesting the minimal sequential transfer of sLP-mCherry to second-recipient neighboring cells. These data demonstrated that a subset of EC population in the liver (such as ECs in zone 1) could be targeted by CILP, which could be used to study the potential communication with their neighboring hepatocytes (Fig. 2*G*).

About half of ECs in the livers of *Mfsd2a-CreER;R26-sLP-mCh* mice were mCherry$^+$ (Fig. 2*H*). FACS isolation and subsequent RNA sequencing analysis revealed that mCherry$^+$ ECs were clearly distinct from the mCherry$^-$ ECs (Fig. 2 *I* and *J*). Specifically, the periportal landmark genes including *Dll4*, *Lama4*, *Msr1*, and *Ltbp4* (4) were up-regulated, whereas the pericentral landmark genes such as *Rspo3*, *Wnt9b*, *Cdh13*, and *Thbd* (4) were down-regulated in mCherry$^+$ ECs (Fig. 2*K*). Further analyses demonstrated that genes involved in angiogenesis, regulation of cell adhesion, and response to growth factor were remarkably up-regulated in mCherry$^+$ ECs, whereas genes associated with extracellular matrix organization, chemotaxis, and tissue morphogenesis were significantly down-regulated in these ECs (Fig. 2*L*). The above data demonstrated that neighboring ECs of Mfsd2a$^+$ hepatocytes could be identified specifically and isolated for further analysis by CILP.

Discussion

Our study reported an in vivo neighboring cell labeling method CILP that recorded the transfer of the membrane-permeable fluorescent protein from specific donor to recipient cells. The term "neighboring" here means both direct cell contact and a close range of distance (like 2-3 hepatocytes here). Indefinite sequential transfer of sLP-mCherry across cells was less likely, as the sLP-mCherry protein can last only 4 days once it is taken up by recipient cells (8). Additionally, our experimental data showed that there was no significant difference in cell labeling between samples collected at different time points, suggesting that indefinite sequential transfer of sLP-mCherry is not likely to occur in our genetic system. Coupled with Cre mouse lines, we envisioned that targeting neighboring cells in a specific niche by CILP would provide a platform to understand intercellular interactions during many biological conditions in a spatiotemporal manner in mice.

Materials and Methods

All mouse studies were approved by the guidelines of the Institutional Animal Care and Use Committee of the Institute of Biochemistry and Cell Biology, Center for Excellence in Molecular Cell Science, Chinese Academy of Sciences. The *R26-sLP-mCh-GFP* and *R26-sLP-mCh* mouse lines were generated by homologous recombination using CRISPR/Cas9. Immunostaining of tissue sections and flow cytometric analysis were performed as previously described (15). Bulk RNA from ECs was evaluated using the Agilent 2100 Bioanalyzer, and the accession number for the RNA-sequencing data is deposited in NCBI Sequence Read Archive: BioProject ID PRJNA895960. Unpaired two-tailed Student's *t* tests were used compare differences between two groups. The null hypothesis was rejected if P was < 0.05.

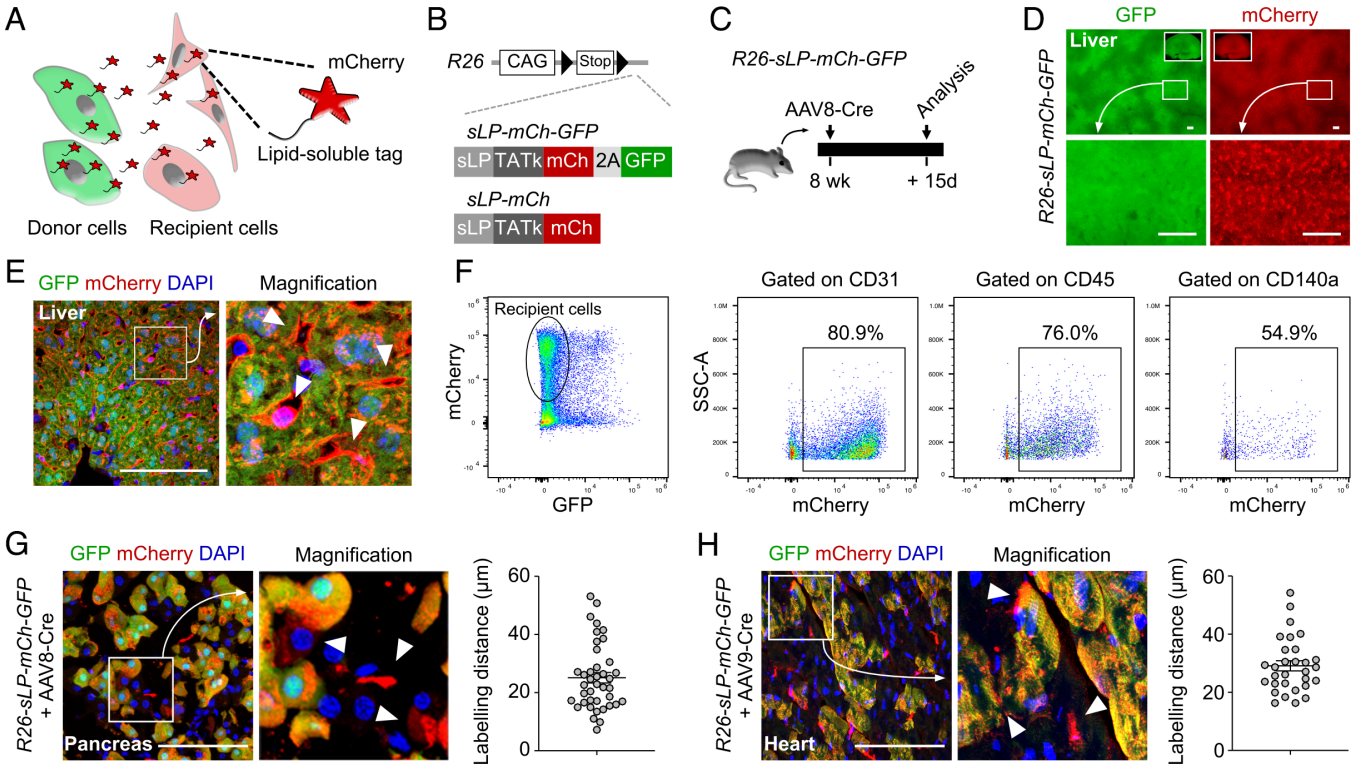

Fig. 1. Generation of CILP for labeling of neighboring cells in vivo. (*A*) Cartoon showing the working principle of CILP. (*B*) Schematic showing generation of *R26-sLP-mCh-GFP* and *R26-sLP-mCh* mice lines. (*C*) Schematic showing the experimental design. (*D*) Whole-mount fluorescence images of livers from *R26-sLP-mCh-GFP* after AAV8-Cre treatment. (*E*) Immunostaining for GFP and mCherry on liver sections from *R26-sLP-mCh-GFP* after AAV8-Cre treatment. Arrowheads, GFP$^-$mCherry$^+$ cells. (*F*) FACS analysis of liver samples from *R26-sLP-mCh-GFP* after AAV8-Cre treatment. (*G* and *H*) Immunostaining for GFP and mCherry on sections of pancreas (*G*) or heart (*H*) samples from *R26-sLP-mCh-GFP* 3 wk after AAV-Cre treatment. Arrowheads, GFP$^-$mCherry$^+$ cells. *Right* panels showing the quantification of labeling distance. n = 40 cells for the pancreas, and n = 30 cells for the heart. Data are representative of 3 mouse samples. (Scale bars, 100 μm.)

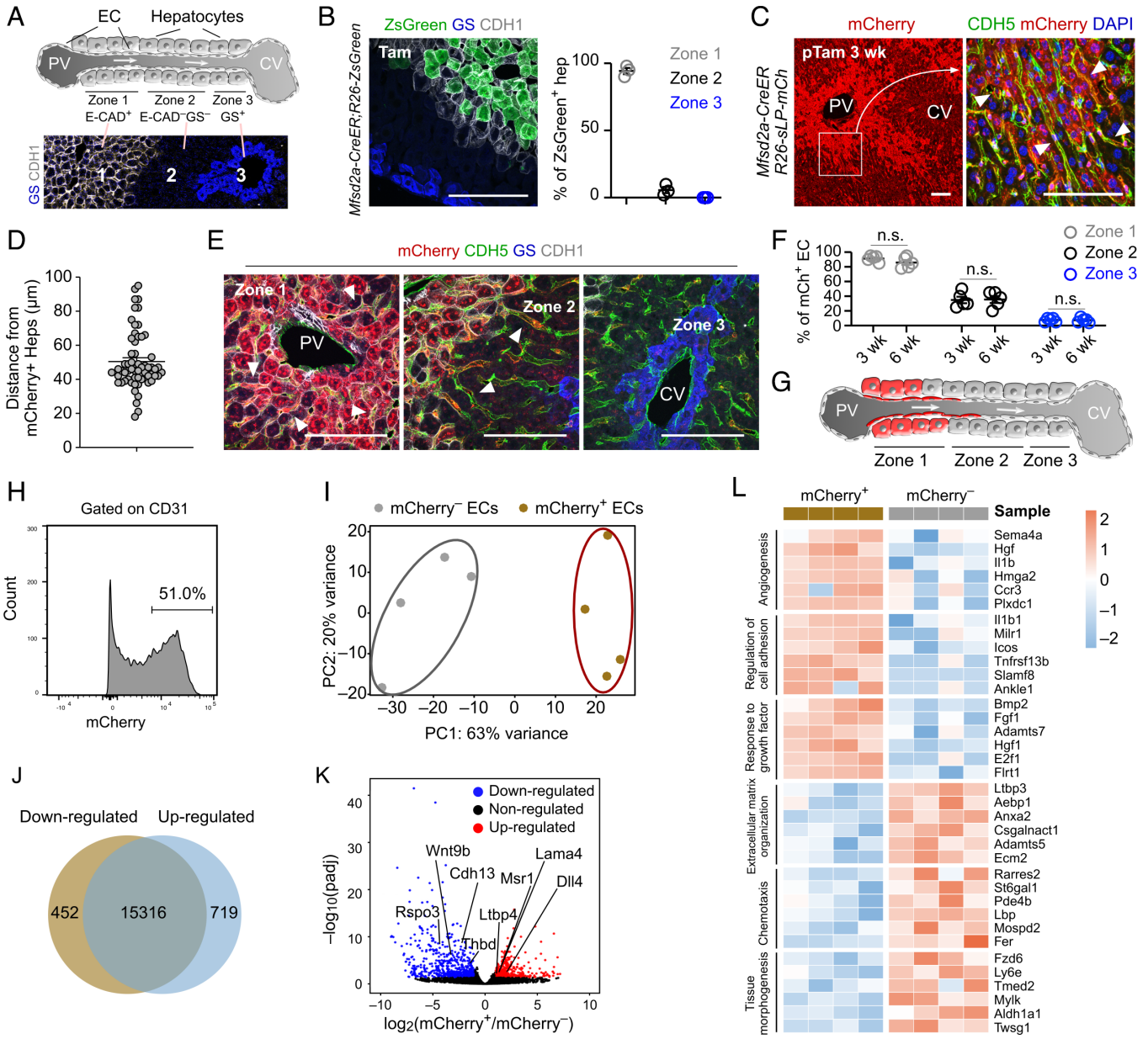

Fig. 2. Identification and characterization of neighboring ECs of Mfsd2a$^+$ hepatocytes. (*A*) Cartoon showing 3 liver zones from the PV (portal vein) to the CV (central vein). The *Lower* panel shows liver sections immunostaining with E-cadherin (CDH1) and glutamine synthetase (GS). (*B*) Immunostaining for CDH1 and GS on liver sections from *Mfsd2a-CreER;R26-ZsGreen* at 2d after tamoxifen treatment. The *Right* panel shows the quantification of the percentage of ZsGreen$^+$ hepatocytes from each zone. n = 3. (*C*) Immunostaining on liver sections from *Mfsd2a-CreER;R26-sLP-mCh* at 3 wk after tamoxifen treatment. Arrowheads, mCherry$^+$CDH5$^+$ ECs. (*D*) Quantification of labeling distance of sLP-mCherry for endothelial cells in livers from (*C*). n = 60 ECs. (*E*) Immunostaining on liver sections from *Mfsd2a-CreER;R26-sLP-mCh* at 3 wk after tamoxifen treatment. Arrowheads, mCherry$^+$CDH5$^+$ ECs. (*F*) Quantification of the mCherry$^+$ ECs for each zone at 3 or 6 wk after tamoxifen treatment. n = 5. (*G*) Cartoon showing the ECs labeled by sLP-mCherry in *Mfsd2a-CreER;R26-sLP-mCh* mice. (*H*) FACS analysis of the percentage of mCherry$^+$ ECs. (*I*) Principal component analysis of endothelial cell signatures. n = 4. (*J*) Venn diagram of differentially expressed genes between mCherry$^+$ and mCherry$^-$ ECs. (*K*) Volcano plot of differentially expressed genes between mCherry$^+$ and mCherry$^-$ ECs. (*L*) Heatmaps of top differentially expressed genes according to Gene Ontology classes. Data are represented as mean ± SEM. n.s., not significant ($P > 0.05$). (Scale bars, 100 μm.)

Data, Materials, and Software Availability. All study data are included in the main text.

ACKNOWLEDGMENTS. This study was supported by the National Key Research & Development Program of China (2019YFA0110403, 2018YFA0108100, 2018YFA0107900, and 2019YFA0802000), NSF of China (31922032, 82088101, 31730112, and 32050087), Shanghai Pilot Program for Basic Research–Chinese Academy of Science, Shanghai Branch (JCYJ-SHFY-2021-0), China Postdoctoral Science Foundation, and the support from the XPLORER PRIZE. We thank Shanghai Model Organisms Center, Inc., for mouse generation.

1. D. T. Scadden, Nice neighborhood: Emerging concepts of the stem cell niche. *Cell* **157**, 41–50 (2014).
2. T. Sato *et al.*, Paneth cells constitute the niche for Lgr5 stem cells in intestinal crypts. *Nature* **469**, 415–418 (2011).
3. J. C. Boisset *et al.*, Mapping the physical network of cellular interactions. *Nat. Methods* **15**, 547–553 (2018).
4. K. B. Halpern *et al.*, Paired-cell sequencing enables spatial gene expression mapping of liver endothelial cells. *Nat. Biotechnol.* **36**, 962–970 (2018).
5. A. Giladi *et al.*, Dissecting cellular crosstalk by sequencing physically interacting cells. *Nat. Biotechnol.* **38**, 629–637 (2020).
6. L. Morsut *et al.*, Engineering customized cell sensing and response behaviors using synthetic notch receptors. *Cell* **164**, 780–791 (2016).

7. G. Pasqual *et al.*, Monitoring T cell-dendritic cell interactions in vivo by intercellular enzymatic labelling. *Nature* **553**, 496–500 (2018).
8. L. Ombrato *et al.*, Metastatic-niche labelling reveals parenchymal cells with stem features. *Nature* **572**, 603–608 (2019).
9. M. Talay *et al.*, Transsynaptic mapping of second-order taste neurons in flies by trans-Tango. *Neuron* **96**, 783–795.e4 (2017).
10. T. H. Huang *et al.*, Tracing neuronal circuits in transgenic animals by transneuronal control of transcription (TRACT). *Elife* **6**, e32027 (2017).
11. S. Cachero *et al.*, BAcTrace, a tool for retrograde tracing of neuronal circuits in Drosophila. *Nat. Methods* **17**, 1254–1261 (2020).
12. M. Flinterman *et al.*, Delivery of therapeutic proteins as secretable TAT fusion products. *Mol. Ther.* **17**, 334–342 (2009).
13. S. Barash, W. Wang, Y. Shi, Human secretory signal peptide description by hidden Markov model and generation of a strong artificial signal peptide for secreted protein expression. *Biochem. Biophys. Res. Commun.* **294**, 835–842 (2002).
14. L. He *et al.*, Proliferation tracing reveals regional hepatocyte generation in liver homeostasis and repair. *Science* **371**, eabc4346 (2021).
15. W. Pu *et al.*, Mfsd2a+ hepatocytes repopulate the liver during injury and regeneration. *Nat. Commun.* **7**, 13369 (2016).